Flexible Three-Axial Force Sensor for Soft and Highly Sensitive Artificial Touch

*Lucie Viry, Alessandro Levi, Massimo Totaro, Alessio Mondini, Virgilio Mattoli, Barbara Mazzolai, and Lucia Beccai**

The emulation of natural touch requires tactile sensors that mechanically comply with the environment – in order to gain relevant information from physical interactions – and that, at the same time, are able to perform when smoothly adapted to host three-dimensional structures.[1,2] For this purpose, successive solutions have been attempted.[3–6] However, to shape deformable materials while developing high precision, yet robust, systems is complex, and it reveals interesting scientific questions in addition to technological challenges.[7,8] As a result, flexible tactile sensors can present a very high pressure sensitivity, but the low saturation level (less than 50 kPa), intrinsically imposed by their architecture and/or manufacturing technology, limits their applications.[4,6,7,9] Moreover, one fundamental function is still being overlooked, and that is the detection of contact force not only in the normal direction to the sensor/object interface, but also in the tangential direction. This would raise the level of encoded information by an artificial touch system closer to natural touch, for instance, slippage and texture detection.[10,11] However, in comparison to pressure sensitive devices, or combined pressure and strain sensors,[12] only a small number of skin-like sensors that can sense normal and tangential forces has been presented in the literature.[13–18] In this context, state-of-the-art developments expose two main challenges: on the one hand, highly sensitive and flexible devices able to detect forces in three dimensions over a large force range are pursued; whereas on the other hand, which is more economically related, their fabrication on large areas is requested. Original alternative sensor designs, using soft materials and processes have been shown to skirt those aspects and/or simplify fabrication processes.[13–15,18–23] Among these, capacitive-based sensors show good potential towards deformable tactile sensors. In particular, Surapaneni et al.[13] have demonstrated very high force range detection (up 320 kPa) and minimum detectable displacement of 60 µm using gold floating electrodes in comb-like structures, whereas other groups, in particular, Noda et al.[14,15,24,25] have introduced original approaches for three-axis force detection using liquid capacitors to address deformability. Here we show the fast and easy fabrication of a fully flexible capacitive three-axial force sensor made with conductive fabric electrodes and an elastomeric material. This unique sensor presented a high compliance, robustness and stability under manipulation and very appealing performances in terms of sensitivity (less than 10 mg and 8 µm, minimal detectable weight and displacement, respectively) and detection range (measured up to 190 kPa, and estimated up to 400 kPa) against the existing state-of-the-art sensors. This work intersects with the recent and exciting direction taken by the research field towards smart, integrated, and flexible electronic devices using an ancestral composite material: textile.[26–29] From less than a decade ago, an increasing number of research efforts have focused on the exploitation of the mechanical properties of textile as a substrate for the absorption or coating of organic and inorganic compounds.[30–32] Whereas conductive fabrics are today already embraced by fashion and architectural designs,[33] the textile platform also opens an original means to develop future electronic and sensing devices.[34] Importantly, this research approach holds promise for the design of soft, small sensing elements, wherever high functional integration and low cost are key elements. We used conductive fabrics to develop and validate an original concept of a small and three-dimensional robust sensor. In this work, we demonstrate that the structuring of the dielectric multilayer and the original combination of materials used gives our sensor the potential to outperform state-of-the-art sensors by employing a fast and accessible yet robust and low-cost fabrication technology. The capacitive sensor is made of two textile electrode levels (i.e., top and bottom) of a non-stretchable copper/tin coated textile (Zelt, Mindset Ltd) separated by a floating fluorosilicone (DowCorning730, 70 µm thickness) film as the dielectric layer (**Figure 1**). Its appealing intrinsic dielectric constant and mechanical properties make fluorosilicone a suitable material for this application. In particular, because of its low adhesion features, an air gap of around 150 µm is naturally formed during fabrication in between the two copper/tin coated textile electrodes. This air gap adds a second dielectric layer to our sensor and triggers very high performances at very low pressures (ca. 0–2 kPa). The woven fabric used in this work presents two main perpendicular sets of conductive yarns (i.e. warp and weft) where the warp yarn is interlaced up and down of the weft yarn creating an opening called shed (see S1, Supporting Information). The volume of air created by the shed contributes to the formation of a third dielectric layer which plays an important role at higher pressures (>2 kPa). This unique composite structure is embedded in between two polydimethylsiloxane (PDMS) packaging layers to form a mechanically flexible and robust capacitive sensor (Figure 1). The sensor design has four square

Dr. L. Viry,[+] Dr. A. Levi,[+] Dr. M. Totaro,[+] Dr. A. Mondini, Dr. V. Mattoli, Dr. B. Mazzolai, Dr. L. Beccai
Center for Micro-BioRobotics
Istituto Italiano di Tecnologia
Viale Rinaldo Piaggio 34, 56025, Pontedera, PI, Italy
E-mail: lucia.beccai@iit.it
[+]These authors contributed equally to this work.

DOI: 10.1002/adma.201305064

ADVANCED MATERIALS
www.advmat.de

www.MaterialsViews.com

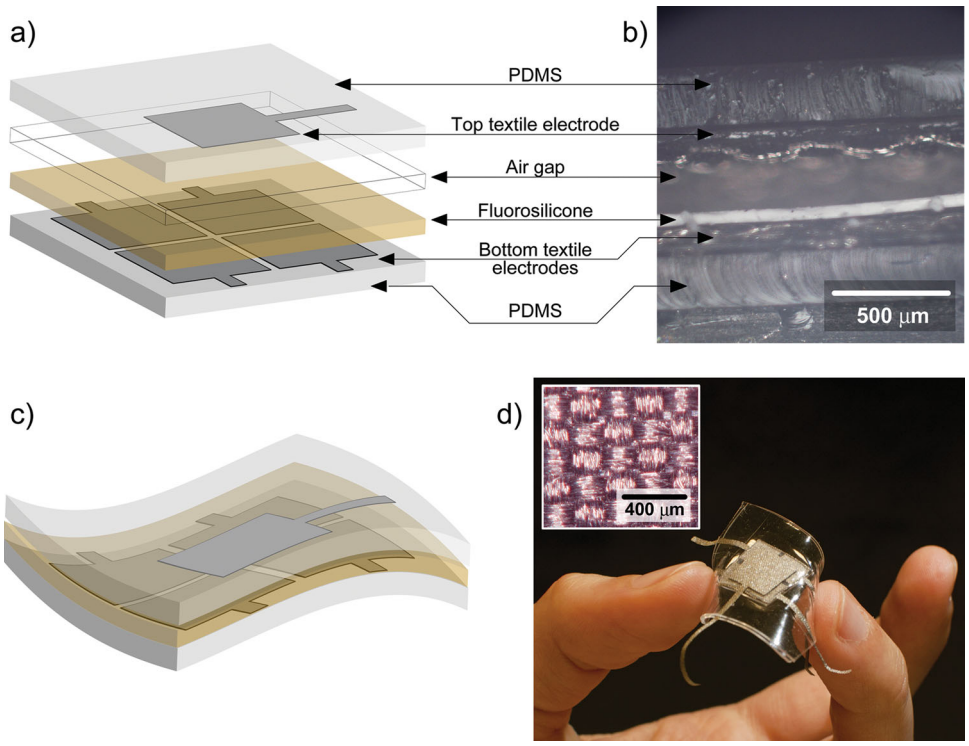

Figure 1. Schematic representation and description of the sensor architecture (a) with corresponding cross-sectional view (b). c,d) Illustration of the flexible sensor. Inset in (d) shows an optical microscopy picture of the conductive textile electrode.

bottom electrodes that form four unit capacitors with a larger common top electrode. The resulting 2D overlapping design of the top electrode on the bottom electrodes is the key to force detection along the three axes.[13,15–17] We consider the parallel-plate capacitor equation $C = \varepsilon_r \varepsilon_0 \frac{A}{h}$ where ε_r, ε_0, A, and h are the relative permittivity of the dielectric material, the vacuum permittivity, the capacitor surface area, and the distance in between the two plates, respectively. When an external force vector $F = \begin{pmatrix} F_x \\ F_y \\ F_z \end{pmatrix}$ is applied, the sensing cell operation is as follows: the normal force component F_z causes a decrease of the distance h between the two electrode levels, thus all four capacitance values increase; whereas the in-plane force components F_x (or F_y) cause the top electrode to slide along the x-axis (or y-axis) affecting the overlapping area between the top and bottom electrodes. As a result, the surface area A of each of the four capacitors is varied. The tactile transduction method of our sensor can be described in space. Specifically, the output signals $\tilde{C}_x$, $\tilde{C}_y$, and $\tilde{C}_z$ are retrieved from the read-out of the four sensor capacitors, as follows:

$$\tilde{C}_x = \frac{1}{4}\left[\frac{\Delta C_1}{C_1^0} + \frac{\Delta C_2}{C_2^0} - \frac{\Delta C_3}{C_3^0} - \frac{\Delta C_4}{C_4^0}\right] \times \left[\frac{1}{1+\tilde{C}_z}\right] \quad (1)$$

$$\tilde{C}_y = \frac{1}{4}\left[-\frac{\Delta C_1}{C_1^0} + \frac{\Delta C_2}{C_2^0} + \frac{\Delta C_3}{C_3^0} - \frac{\Delta C_4}{C_4^0}\right] \times \left[\frac{1}{1+\tilde{C}_z}\right] \quad (2)$$

$$\tilde{C}_z = \frac{1}{4}\left[\frac{\Delta C_1}{C_1^0} + \frac{\Delta C_2}{C_2^0} + \frac{\Delta C_3}{C_3^0} + \frac{\Delta C_4}{C_4^0}\right] \quad (3)$$

where ΔC_1 to ΔC_4 are the capacitance variations measured under an applied load, and C_1^0 to C_4^0 are the reference capacitances measured individually in the absence of load. The factor of ¼ provides the average response of the tactile sensor, which is to be considered when evaluating the sensitivity in each direction. In order to improve the immunity to the intrinsic geometrical mismatch between different electrodes, we consider each normalized relative variation. Indeed, if we were to consider absolute variations – in the case that, for example, one output signal presented a much higher variation than the others – the behavior of the whole sensor would be dominated by this one, affecting the capability to properly distinguish the three force components. Moreover, the normalization of the output signals related to the shear force components needs to be implemented by also taking into account the real initial value of the measurement which is influenced by the initial static normal force that is always present in the experimental protocols implemented in this study (See Experimental details). Effectively, the real tactile experience needs enough friction before generating a tangential displacement. To better approximate this reality, the indentation probe was glued to the top PDMS layer. Moreover, an initial static normal force of, either, 0.5 N or 1 N was applied before securing the plate firmly onto the sensor bottom; hence no pure shear load was applied to the sensor. Indeed, if the device is pressed with an initial normal force, the initial value of each capacitance in average is $C^0\left(1+\tilde{C}_z\right)$. We performed cycling characterizations of the sensor, by statically stimulating it with normal and tangential forces, with the device adapting on both flat and curved surfaces. The normal (F_z), and tangential (F_x, F_y) forces, as well as sensor responses retrieved from Equations (1),

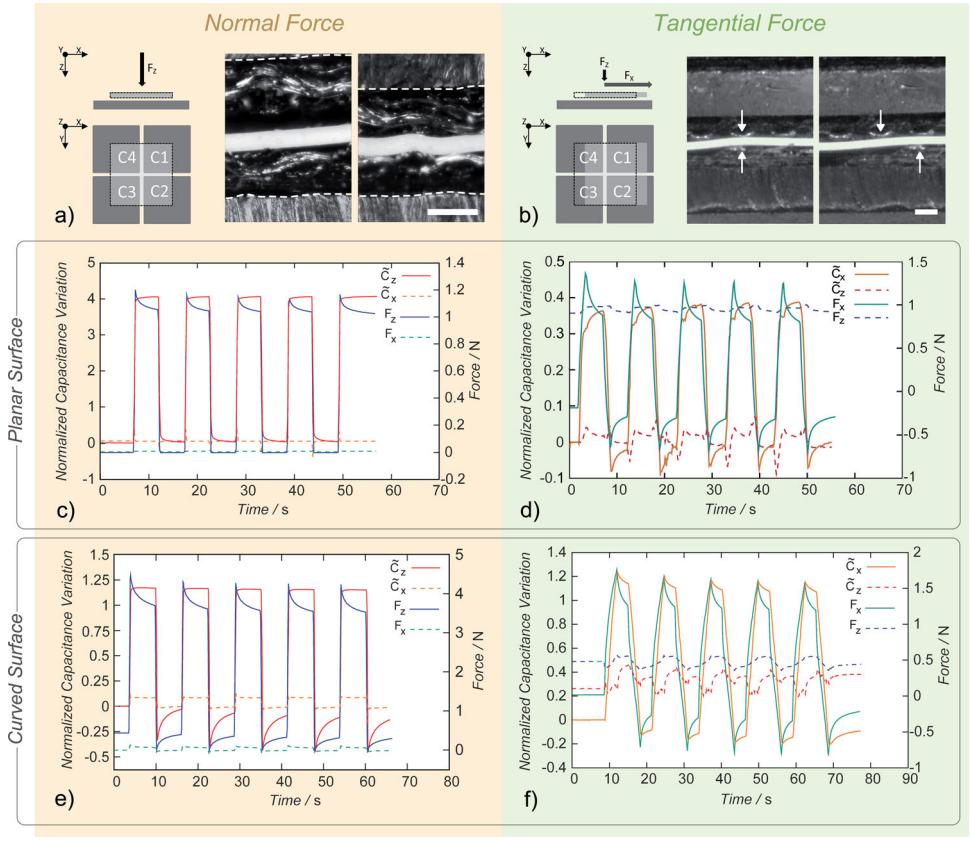

Figure 2. Typical sensor responses to normal and tangential force load–unload cycles. a,b) Sketches and optical microscopy pictures of the sensor's cross section depicting the experimental protocols performed: a) applying forces in the normal direction F_z; b) applying a static normal force and tangential displacement inducing a tangential force stimulation F_x (scale bars: 200 μm). c,d) Responses of the sensor, positioned on a flat surface, to $F_z = 1$ N normal force (c) and to the tangential force F_x produced with a static normal force $F_z = 1$ N and tangential movement (d) (S5, Supporting Information). The same experiments were repeated with the sensor on a 2 cm radius curved surface (e) and (f). Sensor responses related to the perpendicular axis, and due to non-pure axis applied forces are represented in dashed lines.

(2) and (3) are presented in **Figure 2**. We observed a reliable and repeatable behavior of the sensor on both the flat and curved surfaces. As a result of the normal and tangential mechanical stimulation, an instantaneous variation of the output signals was observed (see S3 and S4, Supporting Information). We evaluate that the time response of the device is less than 40 ms, when the maximum sampling rate of 25 Hz is used. Regardless of the limits currently imposed by our electronic system, the proposed sensor shows a very fast response time, when compared to typical touch experiences in nature. For example, in humans mechanoreceptors convey tactile information well within 70 ms,[35] while in plant roots, the time for mechanical stimuli from the soil to deform the natural tissues and elicit internal touch responses is at least 1s.[36] In Figure 2 we show the typical discrimination of the sensor of normal and in-plane forces, confirming that the transduction method used in our sensor is efficient. Additionally, we demonstrate the sensor's ability to independently detect x and y shear forces (see S5, Supporting Information). The viscoelastic nature of the composite materials can be observed during characterization. In particular, the discharge-like behavior measured by the reference load cell (more relevant in Figure 2d, but present also in other cases) is due to the relaxation of the top PDMS layer, which is in direct contact with the probe. However, we note that the sensor's functionality is not affected. The dynamic behavior and performances in the normal and tangential modes were measured and analyzed by observing, with an optical microscope, a cross-section of the sensor positioned on a flat surface (**Figure 3**, see also video S6, Supporting Information). In particular, the performance of the sensor to applied pressures in the range of 0–190 kPa (0–12 N force) is shown in Figure 3a,b. During sensor loading, the distance h between the electrode levels decreases and gives rise to an increase in capacitance. Initially, at very low forces, the thickness of the air dielectric layer is the defining parameter. Up to 32 mN (0.5 kPa), which is the force needed to put the two electrode levels in contact with the fluorosilicone dielectric layer, a very high sensitivity of 14.22 N^{-1} (0.91 kPa^{-1}) is obtained. The capacitance variation for weights of 80, 15, and 10 mg, are shown (Figure 3c), corresponding to average values of ΔC_z of 0.15, 0.05, and 0.025 pF, respectively, measured after contact has been established. Considering that the resolution of the readout electronic system is 1 fF, with an rms noise of about 4 fF, we can reasonably assume a minimal detectable signal of 12 fF (i.e., three times the rms noise). Therefore, the minimal detectable weight of this sensor is less than 10 mg, corresponding to a minimal contact force of less than 0.1 mN. To our knowledge

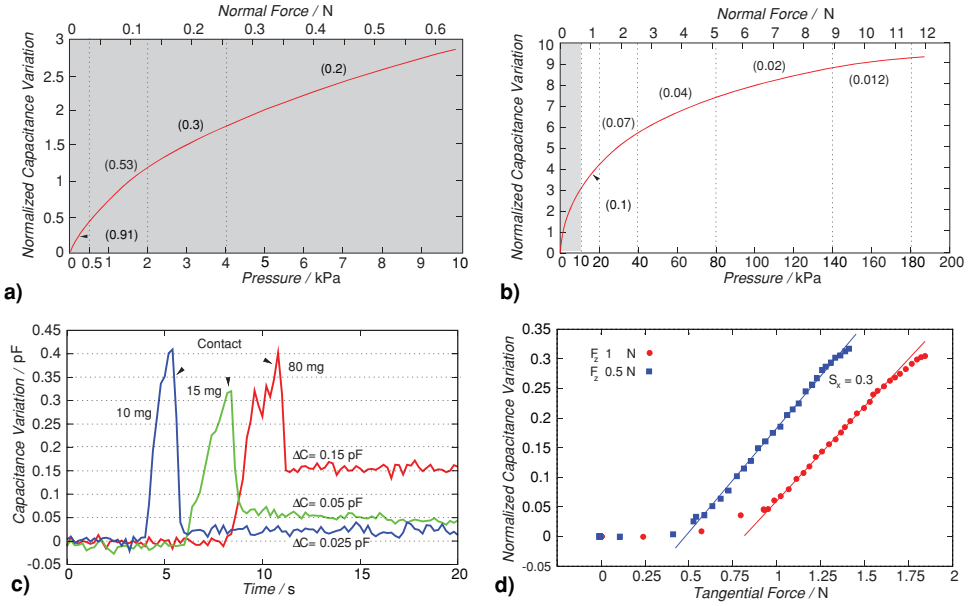

Figure 3. Sensor performances: a,b) Normalized capacitance variation of the sensor versus normal force/pressure in the 0–1 N (0–20 kPa) and the 0–12 N (0–190 kPa) range, respectively. The sensitivity S_z (in kPa^{-1}) is indicated in brackets for different pressure ranges for comparison with the literature. c) Capacitance variation signals for a weight of 80, 15, and 10 mg, corresponding to average values of ΔC of 0.15, 0.05, and 0.025 pF, respectively, after contact. d) Normalized capacitance variation versus the tangential force F_x, in the case of either 0.5 N or 1 N applied static normal force F_z. The sensitivity S_x in the linear region was 0.3 N^{-1}.

these results challenge the sensitivity of today's best examples of flexible pressure sensors, which is around 20 mg[4,18] (see S7, Supporting Information, for an illustrative example of sensor response to light touch). From 32 mN (0.5 kPa) to 640 mN (10 kPa) contact force, the two levels of textile electrodes make contact with the fluorosilicone film, which forms the dielectric layer together with the air volume formed by the shed. As the force increases, the fluorosilicone film complies with the textile surface, thus the shed volume decreases, and hence, the whole air dielectric layer volume decreases (see S1, Supporting Information). In the above force (pressure) range the following sensitivities were obtained (see Figure 3a): 8.28 N^{-1} (0.53 kPa^{-1}) from 32 to 130 mN (0.5–2 kPa); 4.53 N^{-1} (0.30 kPa^{-1}) from 130 to 260 mN (2–4 kPa); and 2.97 N^{-1} (0.20 kPa^{-1}) from 260 mN to 640 mN (4–10 kPa). These results compare very favorably with those achieved by previously reported high-sensitive pressure sensors: 0.55 kPa^{-1} and 0.15 kPa^{-1}, for pressures less than and higher than 2 kPa, respectively;[4] 0.38 kPa^{-1} for pressures higher than 8 kPa.[6] At a force range higher than 640 mN (10 kPa), the sensitivity is expected to be a function of the decrease in the thickness of the fluorosilicone film. Indeed, even at 9 N (140 kPa), no saturation plateau is yet observed, and the sensitivity equals 0.31 N^{-1} (0.02 kPa^{-1}). Reported pressure sensitivity values are: $6.6 \cdot 10^{-4}$ kPa^{-1} for a saturation evaluated around 140 kPa;[16] and, $2.3 \cdot 10^{-4}$ kPa^{-1} for a saturation estimated at 131 kPa.[17] Therefore, these results represent an important improvement over state-of-the-art sensors by two orders of magnitude. Moreover, the pressure (force) vs. normalized capacitance curve is shown in Figure 3b for pressures up to 190 kPa (ca. 12 N), this limit is set by the input dynamics of the readout electronic system. However, it can be seen that the output signal is still well below the saturation, as its slope is around 0.01. An estimation of the sensor saturation can be addressed by a hyperbolic fit of the final part of the curve, also considering that the maximum force detection limit of the sensor is correlated to the mechanical properties of the dielectric material. This way, at 400 kPa (ca. 27 N) (which is the reported fluorosilicone maximum operating stress)[37,38] the estimated sensitivity is 0.0025 kPa^{-1}. Therefore the sensor could still present an improvement for both the saturation level and the pressure sensitivity in comparison to the literature, where a pressure sensitivity of 0.00038 kPa^{-1} for a saturation at 320 kPa[13] has been reported.

Furthermore, in addition to being flexible and mechanically robust over a wide pressure range, the sensor is also able to detect in-plane forces. We investigated the performance of the device under tangential stimulation while applying a static normal force F_z of, either, 0.5 N or 1 N; thus mimicking the tactile indentation needed to induce a tangential force through horizontal displacement (Figure 3d). During the experiments, observations of the cross section under an optical microscope suggest that no shear stress is induced in the dielectric fluorosilicone film and that the top electrode is free to slide over the bottom set of electrodes (see video S6, Supporting Information). In particular, the latter aspect is due to the low friction properties of the fluorosilicone. Independently of the static normal applied force, a 0.4 N tangential force is needed before a significant capacitance variation can be observed (see Figure 3d). This minimum force could reflect the shear strain induced in the thick PDMS layer during the transmission of the tangential displacement. Indeed, such shear force could be needed to initiate the sliding of the top electrode over the bottom electrodes. Then, starting from about 0.4 N, a second regime is observed in which $\tilde{C}_x$ varies linearly with the applied tangential

force. As a higher static normal force must be applied initially to the device, a higher friction force is needed before sliding occurs, and we can observe that, for the same capacitance variation (same overlapping area of the electrodes), doubling the initial load applied to the sensor contributes to a tangential force divided by a factor two. Minimal detected tangential displacements of 8 μm and 14 μm, under 1 N and 0.5 N initial static normal forces, respectively, were evaluated. It should be noted that this result is about one order of magnitude lower than minimal displacements reported in the literature (i.e., 60 μm).[13] Linear behavior is observed within the 0.4–1.2 N and 0.8–1.6 N ranges, for 0.5 N and 1 N static normal forces, respectively. The slope represents the sensitivity of the sensor in the tangential mode. The obtained performances were 0.32 ± 0.02 N^{-1} and 0.34 ± 0.02 N^{-1} for the 0.5 N and 1 N initial contact force curves, respectively. Hence, we may conclude that, due to the design of the sensor, in this regime the tangential sensitivities are almost independent of the normal component of the applied force, and they are equal to about 0.3 N^{-1}. Furthermore, when increasing the tangential force, a deviation of the response from the linear behavior is observed, suggesting that the overlapping area of the electrodes is not dictated by a sliding mechanism of the two sets of electrodes, rather it is limited by the deformable properties of the whole device, in particular its stretchability.

To conclude, the design and the materials used to develop our sensor generate high performing features for the next generation of three-axis soft tactile sensors. Although our design is simple, we have achieved an improved level of tactile information to mimic natural touch. In parallel, the materials used for the multi-layer structure converge in obtaining a soft, flexible and highly sensitive device that offers a low-cost technological approach. New perspectives are thus open for the design of soft and smart interfaces, and for all kinds of applications where natural-like tactile sensing is desired. Importantly, this sensor could target other specific applications than biomimetic touch, in which very low, for instance, heartbeat monitoring (ca. 100 Pa), to very high, for example, foot pressure-distribution monitoring (300–400 kPa), pressure ranges are required. Finally, we expect that the quest for soft and flexible artificial touch systems will steeply increase as soft technological approaches[39] are increasingly being developed in many fields such as exploratory robotics, wearable systems, medicine and rehabilitation, personal robotics, entertainment, and gaming.

Experimental Section

Preparation of Layers: Polydimethylsiloxane (PDMS) (Dow Corning, Sylgard 184; ratio of base to crosslinker, 10:1 by mass) and fluorosilicone (Dow Corning 730) diluted with acetone were degassed and poured on the surface of a silicon wafer previously covered with adhesive tape. After spin-coating and curing at room temperature for around 24 h, membranes of, respectively, 300 μm and 70 μm thickness were obtained. The PDMS membranes were used as external sealing layers whereas the fluorosilicone film was part of the dielectric layering of the sensor. The dielectric constant of DowCorning730 fluorosilicone is 5.5.

Textile-Based Sensor Fabrication: Copper/tin coated woven fabric (Zelt fabric – Mindsets Ltd, UK) with an intrinsic resistance of 50 mΩ $\square^{-1}$ was cut by laser (VLS 3.50; Universal Laser Systems, Inc., USA), with a resolution of around 0.5 mm, into four bottom electrodes of 5 mm × 5 mm and one 8 mm × 8 mm top electrode. The textile electrodes were positioned over the PDMS membranes and maintained in position with double-sided adhesive tape. The two layers were then assembled face to face and the fluorosilicone dielectric membrane was placed in between. An air gap of approximately 150 μm thickness was naturally formed because of the low surface free energy of fluorosilicone. The bottom electrodes and top electrodes were manually centered with respect to each other. As the capacitance measurement was differential, the variation in electrode positioning did not affect the sensor behavior. This fabrication aspect emphasizes the simple, fast, and low-cost technological fabrication process of the sensor.

Experimental Set Up for Measurements: A schematic of the set up is shown in Figure S2 in the Supporting Information. An 8 × 8 mm^2 Delrin ® flat probe was mechanically interfaced to a 6-axis load cell (ATI NANO 17 SI-25-0.25, Apex, NC, USA), which acquired force data during the experiment. The alignment of the load cell to the device was determined with an initial rough manual positioning, by means of three orthogonal manual micrometric translation stages with crossed roller bearings (M-105.10, PI, Karlsruhe, Germany) followed by an accurate controlled positioning, by means of two servo-controlled micrometric translation stages: (M-111.1, PI, Karlsruhe, Germany) for the normal direction (*z*), and (M-126.1 PI, Karlsruhe, Germany) for the shear direction (*x*), respectively. Cyclic indentation (static mode) and force incrementing (dynamic mode) experiments were performed at constant speed. For tangential characterizations, the probe was glued to the device and a static normal force of 0.5 N or 1 N was initially applied before translating the stage in the *x*-direction. In this way, sufficient friction was provided in order to generate a displacement and an overlapping area of top and bottom electrodes, and an experimental protocol that approximates a real tactile event was used. Capacitance measurements were performed by means of custom electronics. Each capacitance output signal was acquired by means of a 24-bit capacitance-to-digital converter (CDC) (AD7747, Analog Devices Inc., Nordwood, MA, USA). The input dynamics of the CDC was 16 pF, which was fully used during sensor characterization. In order to minimize the influence of parasitic capacitances (due to wires, connections, etc), the measuring was done in differential mode, using a dummy reference capacitor for each capacitance channel. In addition, to further reduce parasitic capacitances, the device was connected to the electronic board by means of shielded cables. The capacitance resolution was 1 fF, and, because of the strategies described above, the measured rms noise could be reduced to about 4 fF. Therefore, the minimal detectable signal was about 12 fF (three times larger than the rms noise). Data were acquired by means of a 32-bit PIC micro-controller board (PIC32MX460F512L, Microchip Technology Inc., Chandler, AZ, USA) and sent to a PC via USB. The whole system, comprising the translation stages, the load cell, and the capacitance acquisition board, was connected to a PC. A graphical user interface was implemented to acquire force and capacitance measurements simultaneously, and to control the linear translation stages. In order to determine the initial absolute values needed for normalization, each capacitance was measured in absence of externally applied loads by means of a precision LCR meter (E4980A, Agilent Technologies Inc., Santa Clara, CA, USA). Finally, the sensitivity of the sensor was calculated as the slope of the normalized capacitance variation in function of the force, in different force ranges. For the normal force, the equivalent pressure was considered too and, in the present manuscript, the sensitivity is indicated in kPa^{-1} in order to better compare the resulting data with state-of-the-art sensors in the literature.

Supporting Information

Supporting Information is available from the Wiley Online Library or from the author.

Acknowledgements

This study was partially funded by the PLANTOID project (EU-FP7-FET-Open grant n.: 29343).
Note: The licence of this manuscript was changed after initial online publication, as of May 2, 2014.

Received: October 10, 2013
Revised: December 23, 2013
Published online: February 20, 2014

[1] J. J. Boland, *Nat. Mater.* **2010**, *9*, 790.
[2] B. Y. R. Pfeifer, M. Lungarella, F. Iida, *Commun. ACM* **2012**, *55*, 76.
[3] T. Sekitani, T. Someya, *Adv. Mater.* **2010**, *22*, 2228.
[4] S. C. B. Mannsfeld, B. C. K. Tee, R. M. Stoltenberg, C. V. H. H. Chen, S. Barman, B. V. O. Muir, A. N. Sokolov, C. Reese, Z. Bao, *Nat. Mater.* **2010**, *9*, 859.
[5] M. Kaltenbrunner, T. Sekitani, J. Reeder, T. Yokota, K. Kuribara, T. Tokuhara, M. Drack, R. Schwödiauer, I. Graz, S. Bauer-Gogonea, S. Bauer, T. Someya, *Nature* **2013**, *499*, 458.
[6] G. Schwartz, B. C.-K. Tee, J. Mei, A. L. Appleton, D. H. Kim, H. Wang, Z. Bao, *Nat. Commun.* **2013**, *4*, 1859.
[7] J. A. Rogers, T. Someya, Y. Huang, *Science* **2010**, *327*, 1603.
[8] N. Lu, D.-H. Kim, *Soft Robot.* **2013**, *1*, 53.
[9] K. Takei, T. Takahashi, J. C. Ho, H. Ko, A. G. Gillies, P. W. Leu, R. S. Fearing, A. Javey, *Nat. Mater* **2010**, *9*, 821.
[10] J. Scheibert, S. Leurent, A. Prevost, G. Debrégeas, *Science* **2009**, *323*, 1503.
[11] L. Beccai, S. Roccella, L. Ascari, P. Valdastri, A. Sieber, M. C. Carrozza, P. Dario, *IEEE/ASME Trans. Mechatronics* **2008**, *13*, 158.
[12] D. P. J. Cotton, I. M. Graz, S. P. Lacour, *Proc. Chem.* **2009**, *1*, 152.
[13] R. Surapaneni, Q. Guo, Y. Xie, D. J. Young, C. H. Mastrangelo, *J. Micromech. Microengin.* **2013**, *23*, 075 004.
[14] K. W. Liao, M. T. Hou, J. A. Yeh, in *IEEE Transducers Conf.* **2013**, pp. 1000–1010.
[15] K. Noda, K. Matsumoto, I. Shimoyama, *Sens. Actuators A – Phys.* **2013**, DOI 10.1016/j.sna.2013.09.031.
[16] J. A. Dobrzynska, M. A. M. Gijs, *J. Micromech. Microengin.* **2013**, *23*, 015 009.
[17] H.-K. Lee, J. Chung, S.-I. Chang, E. Yoon, *J. Micromech. Microengin.* **2011**, *21*, 035 010.
[18] C. Pang, G. Y. Lee, T. I. Kim, S. M. Kim, H. N. Kim, S. H. Ahn, K. Y. Suh, *Nat. Mater.* **2012**, *11*, 795.
[19] A. Russo, B. Y. Ahn, J. J. Adams, E. B. Duoss, J. T. Bernhard, J. A. Lewis, *Adv. Mater.* **2011**, *23*, 3426.
[20] X. Wang, T. Li, J. Adams, J. Yang, *J. Mater. Chem. A* **2013**, *1*, 3580.
[21] D. J. Lipomi, M. Vosgueritchian, B. C. Tee, S. L. Hellstrom, J. A. Lee, C. H. Fox, Z. Bao, *Suppl. Inf.* **2011**, 1.
[22] P. Roberts, D. D. Damian, W. Shan, T. Lu, C. Majidi, *IEEE Int. Conf. Robot. Autom.* **2013**, pp. 3514.
[23] M. Ramuz, B. C. K. Tee, J. B. H. Tok, Z. Bao, *Adv. Mater.* **2012**, *24*, 3223.
[24] A. Fassler, C. Majidi, *Smart Mater. Struct.* **2013**, *22*, 055 023.
[25] R. Surapaneni, Y. Xie, K. Park, C. Mastrangelo, *Proc. Eng.* **2011**, *25*, 124.
[26] P. Gould, *Mater. Today* **2003**, 38.
[27] K. Cherenack, L. van Pieterson, *J. Appl. Phys.* **2012**, *112*, 091 301.
[28] "www.proetex.org"
[29] "www.media.mit.edu/wearables/mithril/index.html"
[30] M. Hamedi, L. Herlogsson, X. Crispin, R. Marcilla, M. Berggren, O. Inganäs, *Adv. Mater.* **2009**, *21*, 573.
[31] A. M. Gaikwad, A. M. Zamarayeva, J. Rousseau, H. Chu, I. Derin, D. a Steingart, *Adv. Mater.* **2012**, *24*, 5071.
[32] S. Takamatsu, T. Kobayashi, N. Shibayama, K. Miyake, T. Itoh, *Sens. Actuators A – Phys.* **2012**, *184*, 57.
[33] "www.ifmachines.com"
[34] K. Cherenack, C. Zysset, T. Kinkeldei, N. Münzenrieder, G. Tröster, *Adv. Mater.* **2010**, *22*, 5178.
[35] G. Westling, R. S. Johansson, *Exp. Brain Res.* **1987**, *66*, 128.
[36] G. B. Monshausen, T. N. Bibikova, M. H. Weisenseel, S. Gilroy, *Plant Cell* **2009**, *21*, 2341.
[37] "www.dowcorning.com"
[38] "www.actuatorweb.org"
[39] B. Trimmer, *Soft Robot.* **2013**, *1*, 14.